

Control of orbital angular momentum of light, with optical fibers

Nenad Bozinovic^{1,*}, Steven Golowich², Poul Kristensen³, and Siddharth Ramachandran^{1,*}

¹ Boston University, 8 Saint Mary's Street, Boston, MA, 02215, USA

² MIT Lincoln Laboratory, 244 Wood Street, Lexington, MA, 02420, USA

³ OFS-Fitel, Priorparken 680, Broendby 2605, Denmark

*Corresponding authors: nesa@bu.edu, sidr@bu.edu

Compiled April 30, 2012

We present a fiber-based method for generating vortex beams with a tunable value of orbital angular momentum (OAM) from $-1\hbar$ to $+1\hbar$ per photon. We propose a new method to determine the modal content of the fiber and demonstrate high purity of the desired vortex state (97% after 20 m, even after bends and twists). This method has immediate utility for the multitude of applications in science and technology that exploit vortex light states. © 2012 Optical Society of America

OCIS codes: 050.4865, 060.2340, 060.4230, 140.3300, 260.6042

Because of their ability to carry orbital angular momentum (OAM) [1], vortex beams have generated considerable interest in the recent past, finding applications in the areas of optical tweezers [2, 3], higher dimensional classical and quantum communications [4, 5], atom manipulation [6], and microscopy [7].

The most common methods for vortex beam generation use spatial light modulators (SLM). A fiber-based generation technique, on the other hand, would yield advantages commonly derived from fibers, such as remote delivery and compactness. In addition, the prospect of exploiting fiber nonlinear optical properties [8] would enable temporal and spectral control of vortex beams.

In order to carry OAM, a fiber must support higher-order modes (HOM). Specifically, it can be shown that the linear combination of two HE_{21} HOMs with a $\pm\pi/2$ phase shift between them will result in OAM states [9, 10]. Systems that induce stress in a multimode fiber [11] or utilize acoustic long-period gratings [10] to achieve this $\pi/2$ phase shift have been demonstrated. However, mode coupling in fibers destabilizes the OAM states, leading to multipath interference (MPI) [12, 13]. In most multimode fibers, the TE and TM modes always coexist with the desired HE_{21} modes, and will couple with them to produce linearly polarized (LP) states at the output [14]. Not being true eigenmodes of the fiber, the LP modes cannot carry OAM, and to the best of our knowledge, OAM states have been demonstrated only in short (≤ 30 cm), straight fibers.

In this letter, we show that the OAM states can be created with 97% purity in a 20-m-long fiber, even in the presence of bends and twists. To achieve this, we designed and fabricated a so-called vortex fiber that lifts the degeneracy among the higher order LP_{11} family of modes, thereby minimizing the coupling to the TE and TM modes [14]. Figure 1 shows the experimental setup. Using standard single mode fiber (SMF), a 50-nm-wide 1550-nm LED, and a narrowband CW tunable

laser (Agilent 8168F) were multiplexed into a 20-m-long vortex fiber. Thereafter, using a microbend grating (40-mm length, $475\text{-}\mu\text{m}$ period) [15], with only LED source turned on, we obtained 18-dB of mode conversion from the input fundamental mode to the desired HE_{21}^{odd} mode (see the transmission spectrum in Fig. 1b). Next, we switched the source to the laser, tuned to the resonant mode-conversion wavelength (1527 nm). The vortex fiber is then cleaved approximately 20 m after the output of the microbend grating and imaged onto a camera (VDS, NIR-300, InGaAs).

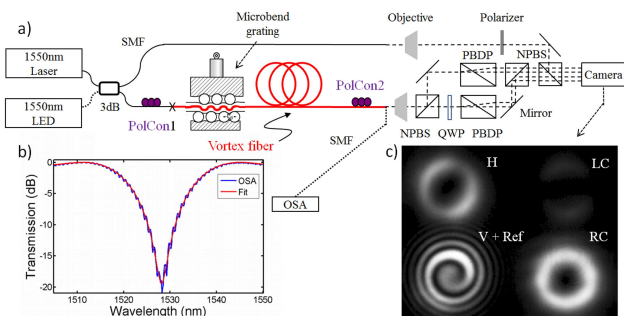


Fig. 1. (Color online) (a) Experimental setup. (b) Grating resonance spectrum used to deduce HE_{21}^{odd} mode conversion level. (c) Camera image showing $l = 1$ OAM, $s = 1$ SAM state.

In order to determine the purity of the vortex states thus obtained, we have developed a new method that analyzes fiber output projections onto left circular (LC) and right circular (RC) polarization states. In addition, to observe the phase of the beam, we interfered a vertical (V) polarization projection with the reference beam. Using a combination of non-polarizing beam splitters (NPBS), quarter wave plates (QWP) and polarizing beam displacing prisms (PBDP), we devised a setup capable of recording these projections in one camera shot. Previously, it was shown that a linear combination of two

$l = \pm 1$ OAM modes will have a total OAM of topological charge that lies between $-1 \leq l \leq 1$. [16]. By adjusting paddles on a commercial polarization controller mounted on our vortex fiber (PolCon2 of Fig. 1a), we were able to tune the output OAM state from $l = -1$ to $l = 1$ (Fig. 1c shows the output of the $l = 1$ OAM and $s = 1$ spin angular momentum (SAM) state).

In general, light at the fiber output can contain contributions from the six vector modes: $\mathbf{HE}_{11}^{x,y}$, $\mathbf{HE}_{21}^{even,odd}$, \mathbf{TM}_{01} and \mathbf{TE}_{01} [9]. To analyze the purity of the OAM states it is more convenient to introduce a so-called vortex basis set:

$$\begin{aligned} \mathbf{V}_{11}^+(r, \theta) &\stackrel{def}{=} (\mathbf{HE}_{11}^x + i\mathbf{HE}_{11}^y)/\sqrt{2} = (\hat{x} + i\hat{y})F_{01}/\sqrt{2} \\ \mathbf{V}_{11}^-(r, \theta) &\stackrel{def}{=} (\mathbf{HE}_{11}^x - i\mathbf{HE}_{11}^y)/\sqrt{2} = (\hat{x} - i\hat{y})F_{01}/\sqrt{2} \\ \mathbf{V}_{21}^+(r, \theta) &\stackrel{def}{=} (\mathbf{HE}_{21}^e + i\mathbf{HE}_{21}^o)/\sqrt{2} = e^{i\theta}(\hat{x} + i\hat{y})F_{11}/\sqrt{2} \\ \mathbf{V}_{21}^-(r, \theta) &\stackrel{def}{=} (\mathbf{HE}_{21}^e - i\mathbf{HE}_{21}^o)/\sqrt{2} = e^{-i\theta}(\hat{x} - i\hat{y})F_{11}/\sqrt{2} \\ \mathbf{V}_T^+(r, \theta) &\stackrel{def}{=} (\mathbf{TM}_{01} - i\mathbf{TE}_{01})/\sqrt{2} = e^{-i\theta}(\hat{x} + i\hat{y})F_{11}/\sqrt{2} \\ \mathbf{V}_T^-(r, \theta) &\stackrel{def}{=} (\mathbf{TM}_{01} + i\mathbf{TE}_{01})/\sqrt{2} = e^{i\theta}(\hat{x} - i\hat{y})F_{11}/\sqrt{2} \end{aligned}$$

where we have used the fact that, for this fiber, the vector modes may be accurately expressed as linear combinations of LP modes through the weak guidance approximation, and $F_{lm}(r)$ denote the radial wave functions of the LP $_{lm}$ modes [9]. Note that in this representation, the \mathbf{V}_{21}^{\pm} modes correspond to the desired OAM states in the fiber. The total electric field can be expressed as:

$$\mathbf{E}(r, \theta) = \sum_{l=[11,21,T]} \sum_{s=[+,-]} \gamma_l^s \mathbf{V}_l^s(r, \theta), \quad (1)$$

where γ_l^s are the mode field complex amplitudes of the vortex basis vectors. We denote mode power contributions as:

$$MPI_l^s \stackrel{def}{=} 10 \log_{10}(|\gamma_l^s|^2 / P_{tot}), \quad (2)$$

where $P_{tot} = \sum_l \sum_s |\gamma_l^s|^2$. To experimentally measure the mode amplitudes, we consider the intensity of the LC polarization projection:

$$|P_+ \mathbf{E}(r, \theta)|^2 = |\gamma_{11}^+ F_{01}(r) + \gamma_{21}^+ e^{i\theta} F_{11}(r) + \gamma_T^+ e^{-i\theta} F_{11}(r)|^2.$$

The key approximation in our analysis is that the $|\gamma_{11}^+||\gamma_T^+|$ term may be neglected, which is valid when most of the power is confined to the \mathbf{HE}_{21} modes, as is the case in the experiments presented below. In addition, for simplicity we confine attention to the points on the radius r_0 , for which $F_{01}(r_0) \approx F_{11}(r_0)$ (we observe that r_0 conveniently corresponds to the radius of the LC and RC projection ring). The LC azimuthal intensity at r_0 now simplifies to:

$$|P_+ \mathbf{E}(r_0, \theta)|^2 \sim DC + \Delta_1 \cos(\theta + \phi_{21,11}) + \Delta_2 \cos(2\theta + \phi_{21,T}), \quad (3)$$

where ϕ_{ij} indicates the phase difference between the two corresponding modes and we define:

$$DC \stackrel{def}{=} |\gamma_{11}^+|^2 + |\gamma_{21}^+|^2 + |\gamma_T^+|^2, \quad (4)$$

$$\Delta_1 \stackrel{def}{=} 2|\gamma_{11}^+||\gamma_{21}^+|, \quad (5)$$

$$\Delta_2 \stackrel{def}{=} 2|\gamma_{21}^+||\gamma_T^+|. \quad (6)$$

By taking the Fourier series of $|P_+ \mathbf{E}(r_0, \theta)|^2$, the coefficients DC , Δ_1 and Δ_2 can be determined; the mode powers ($|\gamma_l^s|^2$) can then be obtained by solving Eq.s 4-6. Figure 2a shows an example of a measurement of $|P_+ \mathbf{E}(r_0, \theta)|^2$ – the azimuthal intensity variation of the image that occurs due to interference between the \mathbf{V}_{21}^+ , \mathbf{V}_{11}^+ and \mathbf{V}_T^+ modes. Figure 2b shows the example of the Fourier series analysis, and Fig. 2c illustrates the powers of the extracted modes. An equivalent procedure was also repeated for the RC projection to calculate amplitudes of the negative helicity modes.

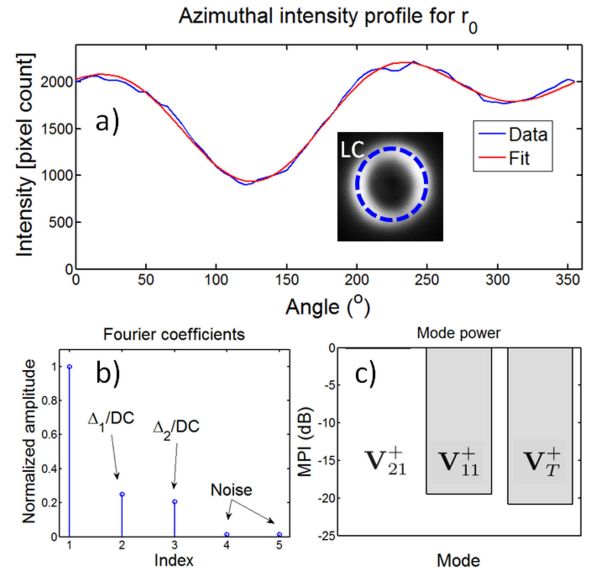


Fig. 2. (Color online) (a) Azimuthal intensity profile of LC projection for radius r_0 . (b) Fourier series coefficients for profile in (a). (c) Extracted modal power contributions.

The high purity of the vortex states implies that only two modes – the $\mathbf{HE}_{21}^{even,odd}$ pair – are dominantly present in the fiber. Here, we would like to emphasize the analogy of the two \mathbf{HE}_{21} modes with the two linearly-polarized fundamental modes – $\mathbf{HE}_{11}^{x,y}$. As with the two fundamental modes, we first note that since the \mathbf{HE}_{21} modes are degenerate, they can easily couple to each other under controlled perturbations. Second, just as a linear combination of two fundamental modes with $\pm\pi/2$ phase shift will create a circularly polarized state, the same linear combination of the two \mathbf{HE}_{21} modes results in an OAM state. This analogy has also been elegantly represented by a higher order Poincaré sphere by other authors studying OAM [17, 18]. A general linear combination of the two $l = \pm 1$ OAM modes will have a topological charge with non-integer total OAM [16].

In order to show the ability of the system to control OAM, camera images were observed and analyzed while the polarization controller (PolCon2 on Fig 1a) was manually tuned using adjustable paddles. Figure 3a shows the modal power distribution as the system was tuned through the different linear combinations of the vortex

states. In particular, Fig. 3b shows observed camera images for the pure \mathbf{V}_{21}^+ state (A), linear combination of the vortex states (B) and the pure \mathbf{V}_{21}^- state (C). Note that using a quarter wave plate, $\mathbf{V}_{21}^{+,-}$ states can be converted to the conventionally constructed linearly polarized OAM states. Our calculation showed that the combined power of the undesired $\mathbf{V}_T^{+,-}$ and $\mathbf{V}_{11}^{+,-}$ modes mostly stayed below a level of -15 dB (3%). In order to estimate the error of the method described, a simulated data set has been created with known contributions of each of the vortex basis vectors (accounting for the dark and shot noise). The data set was then analyzed and the original and the recovered mode powers were compared. Estimated errors were <0.01 dB, ≈ 0.2 dB and ≈ 0.2 dB for the $\mathbf{V}_{21}^{+,-}$, $\mathbf{V}_T^{+,-}$ and $\mathbf{V}_{11}^{+,-}$ modes respectively. With this demonstration we conclude that our system can create any linear combination of OAM states ($-1 \leq l \leq +1$), in a controllable fashion.

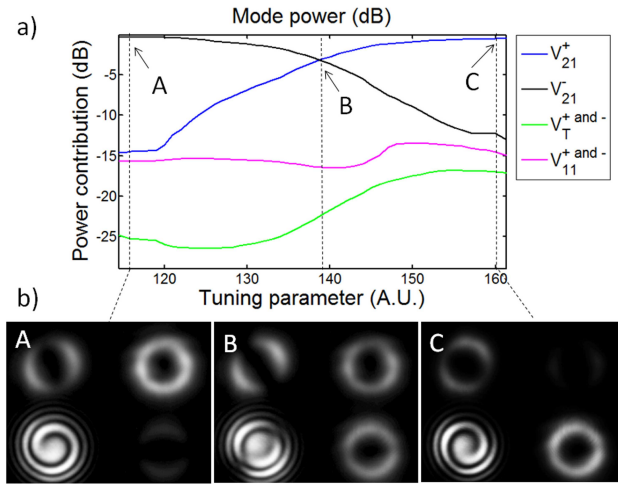


Fig. 3. (Color online) (a) Mode powers as the PolCon2 was adjusted to obtain the desired superposition of the OAM states. (b) Observed camera images at points (A-C).

Having shown arbitrary, controllable preparation of OAM states in a fiber with high purity, we would like to comment on a few experimental limitations of our modal analysis technique. In particular, we noticed that the beam-splitters we used had $\approx 3\%$ transmission difference for s and p polarization, and were slightly birefringent. Both of these factors underestimate the measured vortex mode purity. Since the modal content can be determined by using only two polarization projections, we were able to simplify the setup at the expense of not having the four projections. By doing this, we observed a 6-dB lower power for the $\mathbf{V}_T^{+,-}$ modes, suggesting that the use of better optical components can enable more accurate purity measurements. In addition to the optical components, we noticed that the camera dark noise level introduces a limit for the $\mathbf{V}_{21}^{+,-}$ vortex state sensitivity to be 20 dB. Note that this limit does not apply to the $\mathbf{V}_T^{+,-}$

and $\mathbf{V}_{11}^{+,-}$ modes, as their amplitudes are obtained from the interference effects and not the DC power measurements. We expect that a camera with lower dark-noise count will improve this sensitivity too.

In summary, we demonstrate a novel, all-fiber device, that uses a specialty fiber and a conventional, commercially available fiber polarization controller, to create and tune the OAM of light with a topological charge that could be continuously varied between $-1 \leq l \leq +1$. As a fiber-based system, our device offers flexibility, compactness and portability, unlike free-space optics counterparts. We develop a novel method for modal content recovery and shown that vortex states with high purity can be created (97% after 20-m-long propagation, after bends and twists). This method can find applications in many systems that utilize vortex light states.

We would like to thank P.E. Steinvurzel and P. Gregg for helpful discussions. This work was funded by DARPA grant No. HR0011-11-1-0004.

References

1. L. Allen, M. W. Beijersbergen, R. J. C. Spreeuw, and J. P. Woerdman, *Phys. Rev. A* **45**, 8185 (1992).
2. J. E. Curtis, B. A. Koss, and D. G. Grier, *Opt. Commun.* **207**, 169 (2002).
3. M. K. Kreysing, T. Kiefling, A. Fritsch, C. Dietrich, J. R. Guck, and J. A. Käs, *Opt. Express* **16**, 16984 (2008).
4. G. Gibson, J. Courtial, M. Padgett, M. Vasnetsov, V. Pas'ko, S. Barnett, and S. Franke-Arnold, *Opt. Express* **12**, 5448 (2004).
5. A. Vaziri, G. Weihs, and A. Zeilinger, *Phys. Rev. Lett.* **89**, 240401 (2002).
6. J. W. R. Tabosa and D. V. Petrov, *Phys. Rev. Lett.* **83**, 4967 (1999).
7. S. W. Hell and J. Wichmann, *Opt. Lett.* **19**, 780 (1994).
8. S. Ramachandran, C. Smith, P. Kristensen, and P. Balling, *Opt. Express* **18**, 23212 (2010).
9. A. Snyder and J. D. Love, *Optical Waveguide Theory* (Springer, 1983).
10. P. Z. Dashti, F. Alhassen, and H. P. Lee, *Phys. Rev. Lett.* **96**, 043604 (2006).
11. D. McGloin, N. B. Simpson, and M. J. Padgett, *Appl. Opt.* **37**, 469 (1998).
12. S. Ramachandran, J. Nicholson, S. Ghalimi, and M. Yan, *IEEE Photonics Tech. Lett.*, **15**, 1171 (2003).
13. R. Olshansky, *Appl. Opt.* **14**, 935 (1975).
14. S. Ramachandran, P. Kristensen, and M. F. Yan, *Opt. Lett.* **34**, 2525 (2009).
15. J. N. Blake, B. Y. Kim, H. E. Engan, and H. J. Shaw, *Opt. Lett.* **12**, 281 (1987).
16. C. H. J. Schmitz, K. Uhrig, J. P. Spatz, and J. E. Curtis, *Opt. Express* **14**, 6604 (2006).
17. M. J. Padgett and J. Courtial, *Opt. Lett.* **24**, 430 (1999).
18. G. Milione, H. I. Sztul, D. A. Nolan, and R. R. Alfano, *Phys. Rev. Lett.* **107**, 053601 (2011).

References

1. L. Allen, M. W. Beijersbergen, R. J. C. Spreeuw, and J. P. Woerdman, "Orbital angular momentum of light and the transformation of laguerre-gaussian laser modes," *Phys. Rev. A* **45**, 8185–8189 (1992).
2. J. E. Curtis, B. A. Koss, and D. G. Grier, "Dynamic holographic optical tweezers," *Optics Communications* **207**, 169 – 175 (2002).
3. M. K. Kreysing, T. Kießling, A. Fritsch, C. Dietrich, J. R. Guck, and J. A. Käs, "The optical cell rotator," *Opt. Express* **16**, 16984–16992 (2008).
4. G. Gibson, J. Courtial, M. Padgett, M. Vasnetsov, V. Pas'ko, S. Barnett, and S. Franke-Arnold, "Free-space information transfer using light beams carrying orbital angular momentum," *Opt. Express* **12**, 5448–5456 (2004).
5. A. Vaziri, G. Weihs, and A. Zeilinger, "Experimental two-photon, three-dimensional entanglement for quantum communication," *Phys. Rev. Lett.* **89**, 240401 (2002).
6. J. W. R. Tabosa and D. V. Petrov, "Optical pumping of orbital angular momentum of light in cold cesium atoms," *Phys. Rev. Lett.* **83**, 4967–4970 (1999).
7. S. W. Hell and J. Wichmann, "Breaking the diffraction resolution limit by stimulated emission: stimulated-emission-depletion fluorescence microscopy," *Opt. Lett.* **19**, 780–782 (1994).
8. S. Ramachandran, C. Smith, P. Kristensen, and P. Balling, "Nonlinear generation of broadband polarisation vortices," *Opt. Express* **18**, 23212–23217 (2010).
9. A. Snyder and J. D. Love, *Optical Waveguide Theory* (Springer, 1983).
10. P. Z. Dashti, F. Alhassen, and H. P. Lee, "Observation of orbital angular momentum transfer between acoustic and optical vortices in optical fiber," *Phys. Rev. Lett.* **96**, 043604 (2006).
11. D. McGloin, N. B. Simpson, and M. J. Padgett, "Transfer of orbital angular momentum from a stressed fiber-optic waveguide to a light beam," *Appl. Opt.* **37**, 469–472 (1998).
12. S. Ramachandran, J. Nicholson, S. Ghalmi, and M. Yan, "Measurement of multipath interference in the coherent crosstalk regime," *Photonics Technology Letters, IEEE* **15**, 1171 –1173 (2003).
13. R. Olshansky, "Mode coupling effects in graded-index optical fibers," *Appl. Opt.* **14**, 935–945 (1975).
14. S. Ramachandran, P. Kristensen, and M. F. Yan, "Generation and propagation of radially polarized beams in optical fibers," *Opt. Lett.* **34**, 2525–2527 (2009).
15. J. N. Blake, B. Y. Kim, H. E. Engan, and H. J. Shaw, "Analysis of intermodal coupling in a two-mode fiber with periodic microbends," *Opt. Lett.* **12**, 281–283 (1987).
16. C. H. J. Schmitz, K. Uhrig, J. P. Spatz, and J. E. Curtis, "Tuning the orbital angular momentum in optical vortex beams," *Opt. Express* **14**, 6604–6612 (2006).
17. M. J. Padgett and J. Courtial, "Poincaré-sphere equivalent for light beams containing orbital angular momentum," *Opt. Lett.* **24**, 430–432 (1999).
18. G. Milione, H. I. Sztul, D. A. Nolan, and R. R. Alfano,

"Higher-order poincaré sphere, stokes parameters, and the angular momentum of light," *Phys. Rev. Lett.* **107**, 053601 (2011).